

Supporting Information

Tuning the Electrochemical Redox Mediated Mechanism
of Oxygen Evolution Catalysis on Cobalt sites by
Hydroxide ions Coupling

Wenjuan Song,^{1#} Xiaoyue Duan,^{1#} Poe Ei Phyu Win,¹ Xiang Huang,^{3} Jiong Wang^{1,2*}*

¹Innovation Center for Chemical Science, College of Chemistry, Chemical
Engineering and Materials Science, Soochow University, Suzhou 215006, P. R. China

²Jiangsu Key Laboratory of Advanced Negative Carbon Technologies, Soochow
University, Suzhou 215123, P. R. China

³Quantum Science Center of Guangdong-Hong Kong-Macao Greater Bay Area
(Guangdong), Shenzhen 518045, China

E-mail: huangxiang@quantumsc.cn (X. H.); wangjiong@suda.edu.cn (J. W.)

1. Experiments

Chemicals. P_2O_5 , $K_2S_2O_8$, $Co(NO_3)_2 \cdot 6H_2O$ and 2, 2'-bipyridine, mercaptoacetic acid, benzylthiol, thioanisole, thioacetamide were purchased from Macklin company. Graphite powders and $KMnO_4$ were purchased from Alfa Aesar company. All the used solvents are of analytical grade and used without further purification.

Synthesis of Electrocatalysts. Graphite powders (2 g) were mixed with $K_2S_2O_8$ (1 g) and P_2O_5 (1.2 g) in 98% H_2SO_4 (20 mL), and heated at 100 °C for 10 h. The resultant solids were then dispersed in 98% H_2SO_4 (50 mL) with slowly adding $KMnO_4$ (6.5 g) to react at 50 °C for 6 h, afterwards washed with 3.7% HCl. The final solids were dialyzed for at least 7 days to achieve the precursor of graphene oxides (GO). To synthesize various heteroatoms doped graphene, GO (20 mg) and thioacetamide (1 g) were mixed (~ 1:50, mass ratio) in water/ethanol (10 mL/2.5 mL) solvents under the ultrasonication. Then the suspension was transferred into a polytetrafluoroethylene (PTFE) lined stainless steel autoclave. It was sealed and kept at 150 °C for 3.5 h, and then washed with water and ethanol to obtain S-doped graphene (S_1G). As the control samples, other heteroatoms doped graphene, including S_2G , S_3G , S_4G , NG and G, was synthesized following the same processes as the case of S_1G , except that the precursors were replaced by GO-mercaptoacetic acid (~ 1:50, mass ratio), GO-benzylthiol (~ 1:50, mass ratio), GO-thioanisole (~ 1:50, mass ratio), GO-urea (~ 1:50, mass ratio) and GO, respectively.

To synthesize various molecular cobalt complexes, $Co(NO_3)_2 \cdot 6H_2O$ (2.62 g, 0.009 mol, dissolved in 50 mL methanol) was slowly mixed with 2, 2'-bipyridine (1.41 g, 0.009 mol, dissolved in 50 mL methanol) under stirring. The mixed solution was heated at 60 °C for 2 h under stirring. Afterwards, methanol was removed by rotary evaporation. The resultants were successively washed with acetone, and a small volume of H_2O to get pink compounds, which is denoted as CoN_2 . The single crystal of CoN_2 is grown by dissolving in *N,N*-dimethylformamide (DMF) for slow evaporation at 60 °C, 1 atm. For comparison, CoN_4 and CoN_6 complexes were synthesized following the same processes as the case of CoN_2 , except that the molar ratios of $Co(NO_3)_2 \cdot 6H_2O$ to 2, 2'-

bipyridine were changed to 1:2 and 1:3, respectively. In order to achieve heterogenized Co complexes, CoN₂ complexes were mixed with S₁G, S₂G, S₃G, S₄G, NG and G (mass ratio at 1:1) in DMF, respectively, and were heated at 80 °C for 12 h, 1 atm. The final solids (3 mg) were washed with ethanol, and dispersed in 2 mL isopropanol. The as-obtained products are denoted as S₁G-CoN₂, S₂G-CoN₂, S₃G-CoN₂, S₄G-CoN₂, NG-CoN₂ and G-CoN₂ respectively.

Electrochemical measurements. All the electrochemical measurements were conducted using a CHI 1140 potentiostat with a conventional three-electrode system at ambient environments (~26 °C, 1 atm). The electrocatalyst was coated on the surface of glassy carbon electrode with a diameter of 5 mm to serve as the working electrode, which was connected to the Pine rotation instrument. A Hg/HgO drop soaked in 1 M KOH was applied as the reference electrode and a graphite rod was applied as the counter electrode, respectively. The electrolyte was KOH aqueous solution. According to $E \text{ (vs. RHE)} = E \text{ (vs. Hg/HgO)} + 0.098 + 0.592 \times (\text{pH})$, the electrode potential is converted to reversible hydrogen electrode scale. The applied potentials were corrected for iR_s compensation based on the equation, $E_{\text{corrected}} = E_{\text{applied}} - iR_s \times 0.95$.

Physical Characterizations. The morphology of each sample was characterized by scanning electron microscopy (SEM, Hitachi SU8010). All the samples were observed directly without Au coating. Ultraviolet-visible (UV-vis) spectra were recorded in the 250-400 nm range using a precision cuvette (1 cm path length) on a Shimadzu UV-1900i UV-vis spectrometer. X-ray photoelectron spectra (XPS) were conducted on an EXCALAB 250 XI X-ray photoelectron spectrometer (Thermo Scientific) with monochromatic XPS sensitivity: Ag3d_{5/2} (FWHM≤0.6eV) intensity greater than 10⁶ CPS. Powder X-ray diffraction (XRD) patterns were collected on a Bruker D8 advance instrument with Cu K- α radiation ($\lambda=1.54 \text{ \AA}$) at a generator voltage of 40 kV and a generator current of 50 mA. Electron spin resonance (ESR) spectra were collected on a the JES-X320 ESR spectrometer with a micro-frequency of 9.16 GHz. High resolution transmission electron microscope (HR-TEM) images WERE taken on a Talos F200X (Thermofishe) at 200 kV. Aberration corrected high-angle annular darkfield scanning

transmission electron microscopic (AC HAADF-STEM) images were recorded on the JEOL JEM-2100F at 200 kV. The X-ray absorption fine structure (XAFS) spectrum was recorded at the W1b1 station of the Shanghai Light Source (SSRF) in China, operating at 250GeV, 250mA. The Faraday efficiency (FE) test of O₂ is carried out in the H-type electrolytic cell separated by an ion exchange membrane using the CHI 1140 electrochemical workstation, and the gas products produced in the reaction process are detected online by gas chromatography (Agilent 8890). Nitrogen as the carrier gas, and 1 M KOH as the electrolyte. Raman spectroscopy study was performed using a Renishaw LabRAM HR800 Raman spectrometer equipped with 532 and 633 nm solid-state lasers, 5×, 20×, 50×, and 100× objectives, and a MS 20 Encoded Stage. The measurements used 532 or 633 nm lasers were taken with a range of 100-3500 cm⁻¹ using a 50× long distance objective, 10 s of exposure time, 5% of power, and 3 accumulations. The in situ attenuated total reflectance-fourier transform infrared spectroscopy (ATR-FTIR) study was conducted on a Nicolet iS50 FTIR spectrometer, which was equipped with an MCT detector cooled with liquid nitrogen and the PIKE VeeMAX III variable-angle ATR sampling accessory. In all the measurements, background spectra were collected when a device set up. FTIR spectra were obtained from an average of 64 scans with a resolution of 4 cm⁻¹. The potential dependent spectra were collected by applying the working potential from 1 to 1.7 V vs. RHE in 1 M KOH with steps and durations of 0.1 V and 200 s, respectively. The metal content of each sample was determined by inductively coupled plasma optical emission spectroscopy (ICP-OES). i) For analysis of total metal contents in the each electrocatalyst, samples were digested in a concentrated acid mixture containing 98% H₂SO₄ and 65% HNO₃ (V/V=1/1). The mixed solution was heated at 110 °C for 24 h, and were tested by ICP-OES. ii) For analysis of surface metal contents on the working electrodes, the metal coated electrodes were immersed into 65% HNO₃ for 0.5 min at the ambient condition, and were tested by ICP-OES.

Computational methods. Spin-polarized density functional theory calculations are conducted at the generalized gradient approximation level of theory using the plane-wave mode¹ as implemented in the GPAW code² and atomic simulation environment (ASE).³ The exchange-correlation potential is described using the BEEF-vdW

functional,⁴ and the cutoff energy for the plane-wave basis is set to 600 eV. The Fermi level is smeared using the Fermi-dirac method with a width of 0.05 eV. The vacuum distance is set to be greater than 11 Å, which has been verified as sufficient to decouple interactions between neighboring images. The Brillouin zone is sampled using a k-grid of 1×1×2. The atoms are fully relaxed until the force on each atom is less than 0.05 eV/Å. The reaction free energy for proton-electron coupled electrochemical step is calculated using the computational hydrogen electrode (CHE) model.⁵ The binding energies of *OOH, *O, and *OH are defined in eqs 1-3.

$$\Delta E_{*OOH} = E_{*OOH} + \frac{3}{2}E_{H_2} - 2E_{H_2O} - E_{sub} \quad (1)$$

$$\Delta E_{*O} = E_{*O} + E_{H_2} - E_{H_2O} - E_{sub} \quad (2)$$

$$\Delta E_{*OH} = E_{*OH} + \frac{1}{2}E_{H_2} - E_{H_2O} - E_{sub} \quad (3)$$

The calculated binding energy is converted into Gibbs free energy by applying corrections of 0.4, 0.05, and 0.35 eV for ΔE_{*OOH} , ΔE_{*O} , and ΔE_{*OH} , respectively. These corrections account for contributions from zero-point energy and entropy.⁶ In addition, the solvent stabilization of -0.3 eV is considered for *OH and *OOH due to the hydrogen bonding with water in solution, which is consistent with the previous studies.^{6, 7}

2. Additional Results

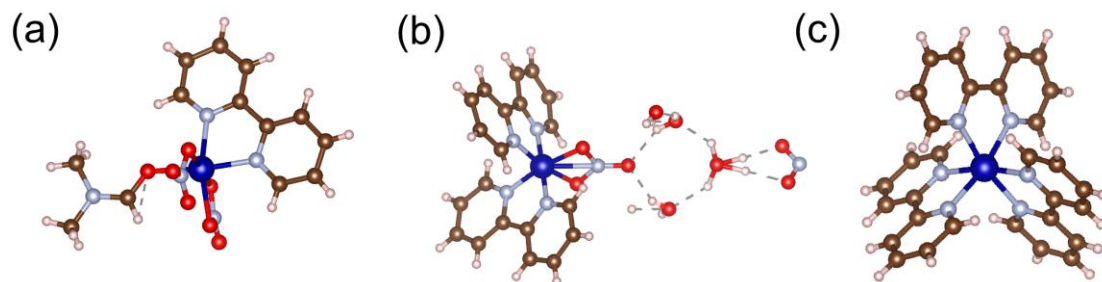


Figure S1. The molecular structures of CoN_2 (a), CoN_4 (b) and CoN_6 (c) complexes detected by X-ray single crystal diffractions. The brown, light blue, blue, red and white spheres represent C, N, Co, O, and H atoms, respectively.

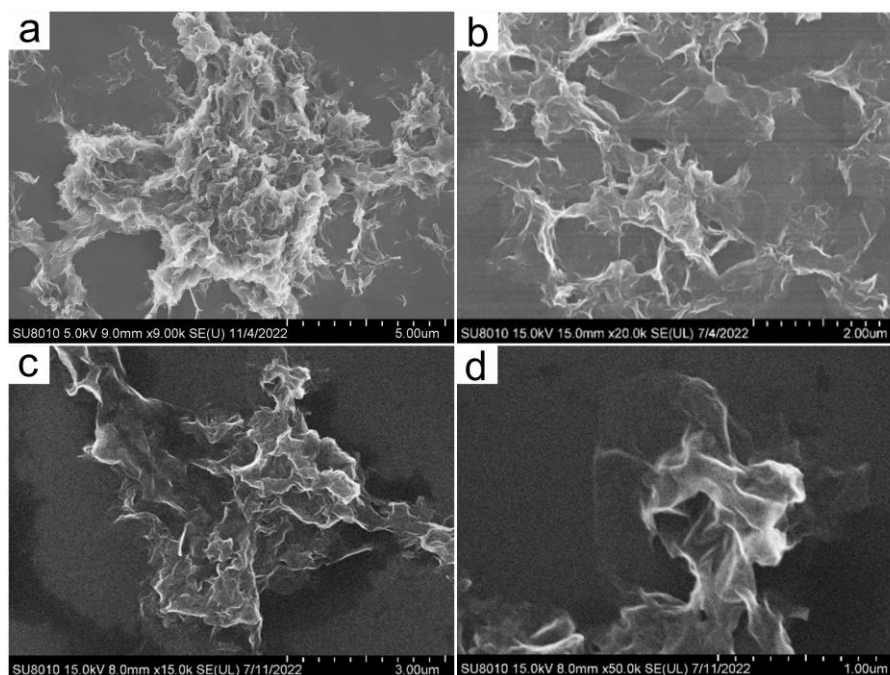


Figure S2. SEM images of S_1G (a, b) and $\text{S}_1\text{G-CoN}_2$ (c, d) at different resolutions.

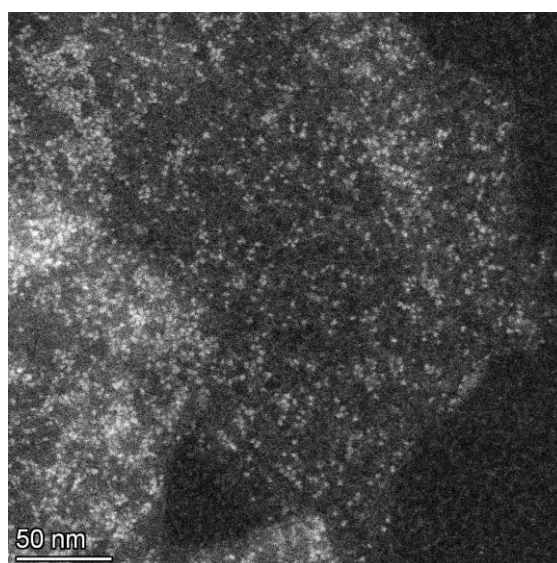


Figure S3. A representative AC HAADF-STEM overall image of S_1G-CoN_2 .

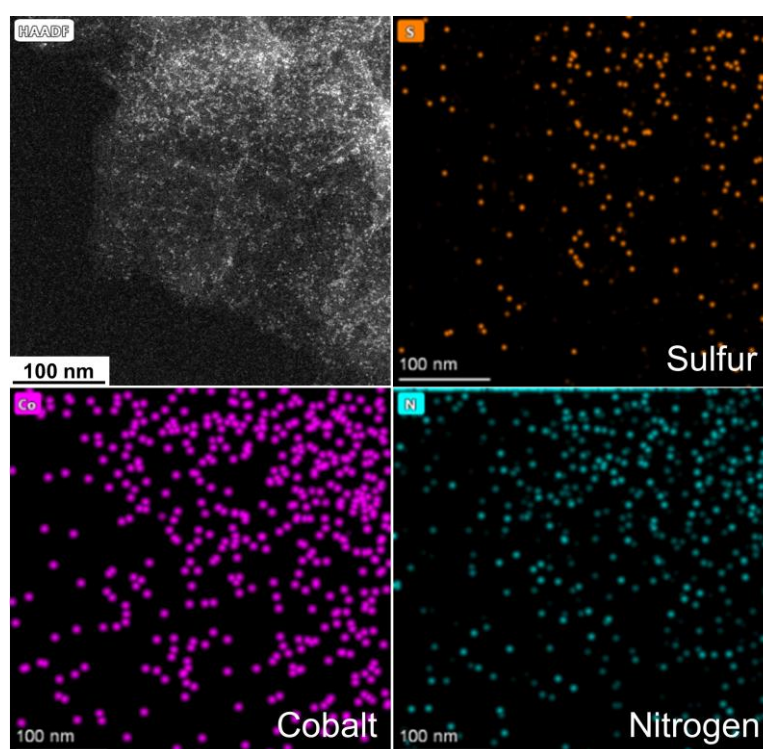


Figure S4. An AC HAADF-STEM image of S_1G-CoN_2 in the dark field mode and the corresponding elemental mapping images by EDS analysis.

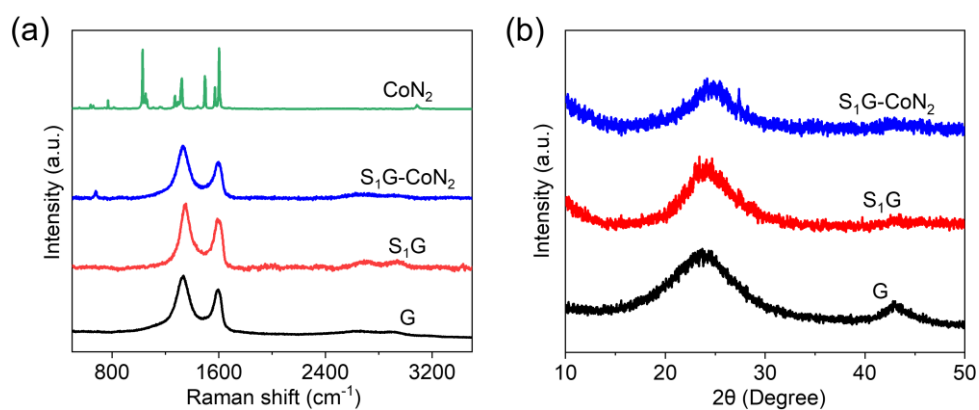


Figure S5. Raman spectra (a) and XRD patterns (b) of pristine G, S₁G and S₁G-CoN₂. The Raman laser is 633 nm. A Raman peak is observed at 682 cm⁻¹ in S₁G-CoN₂ is assigned to the vibrational mode of the Co-O bonds.⁸

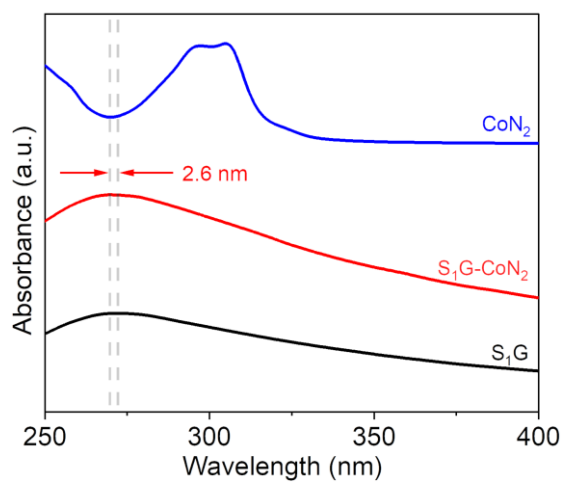


Figure S6. UV-Vis spectra of S₁G-CoN₂, S₁G and CoN₂ collected in isopropanol.

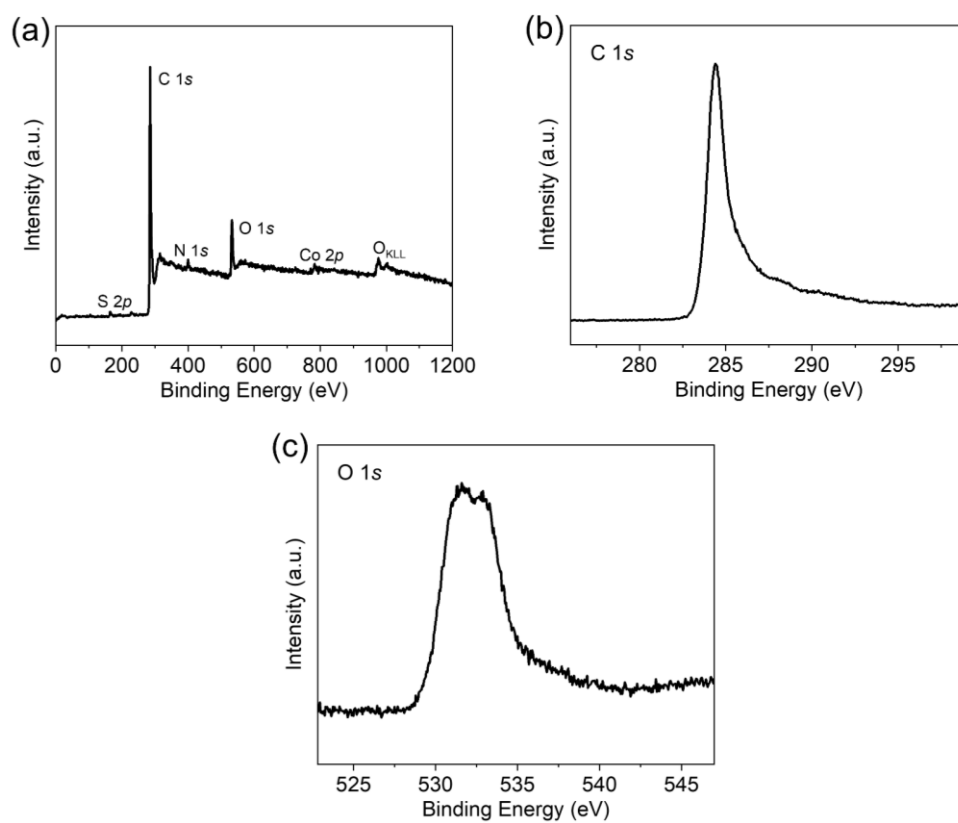


Figure S7. XPS surveys of full elements (a), C *1s* (b) and O *1s* (c) core electron levels of S₁G-CoN₂.

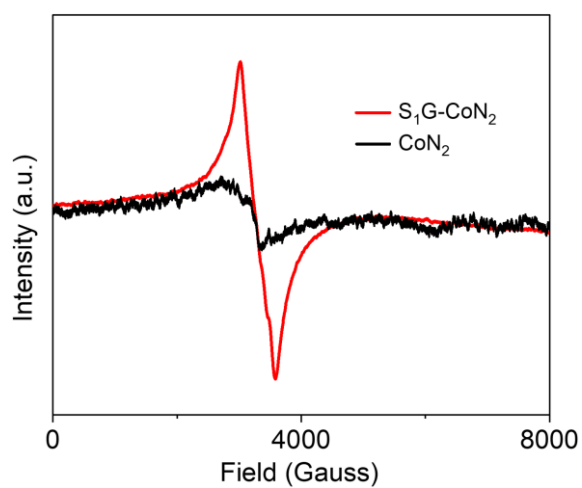


Figure S8. EPR data of S_1G-CoN_2 and CoN_2 collect at the room temperature.

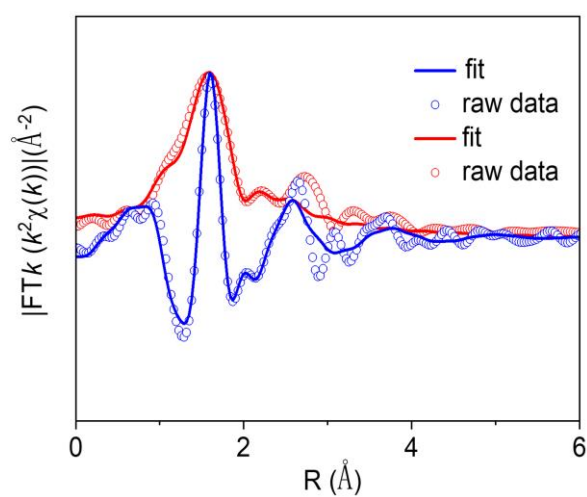


Figure S9. k^2 -weighted Co K-edge FT EXAFS spectra of S_1G-CoN_2 (red) and CoN_2 (blue) in R space.

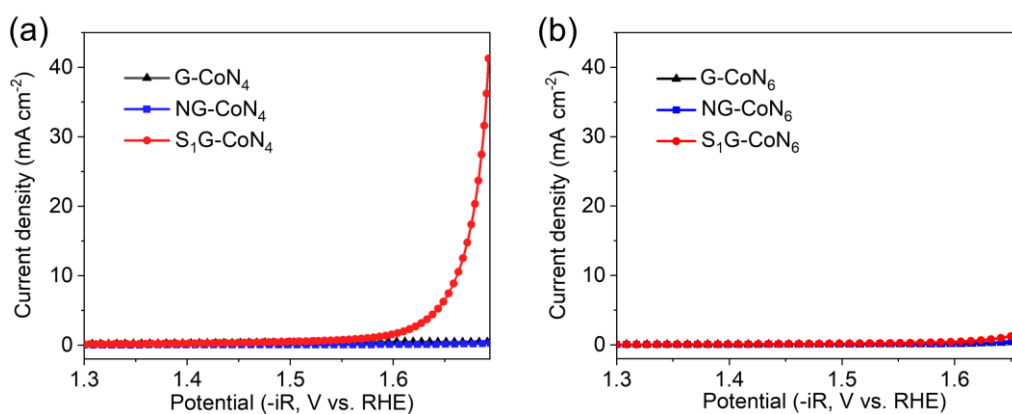


Figure S10. (a) LSVs of G-CoN₄, NG-CoN₄ and S₁G-CoN₄. (b) LSVs of G-CoN₆, NG-CoN₆ and S₁G-CoN₆. 1 M KOH, 10 mV s⁻¹ scan rate, 1600 rpm. The potentials were compensated by 95% iR loss.

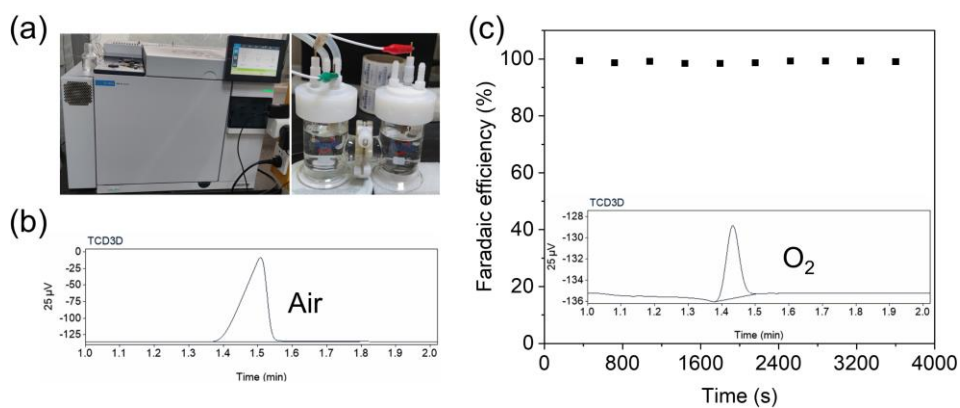


Figure S11. (a) Digital photos of a gas chromatograph and an electrolysis cell for the FE test. (b) The GC data of air. (c) The FEs of O₂ production by S₁G-CoN₂ at different reaction time at a current density of 10 mA cm⁻². The inset shows a representative GC data of O₂ product measured during the OER on S₁G-CoN₂.

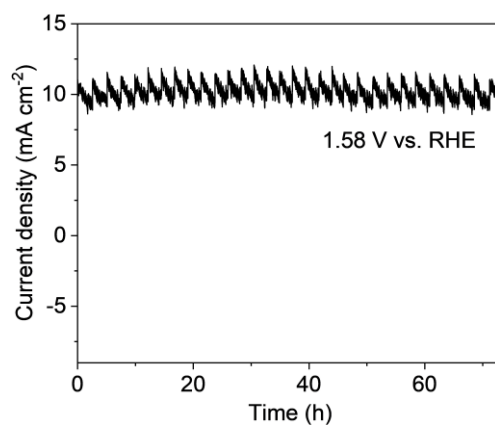


Figure S12. A chronoamperometric curve of S₁G-CoN₂ recorded at 1.58 V vs. RHE in 1 M KOH.

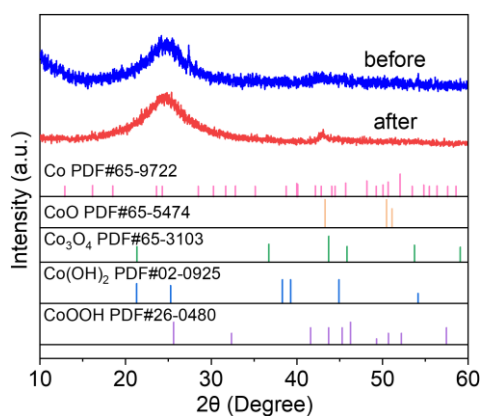


Figure S13. XRD patterns of S₁G-CoN₂ before and after the stability test.

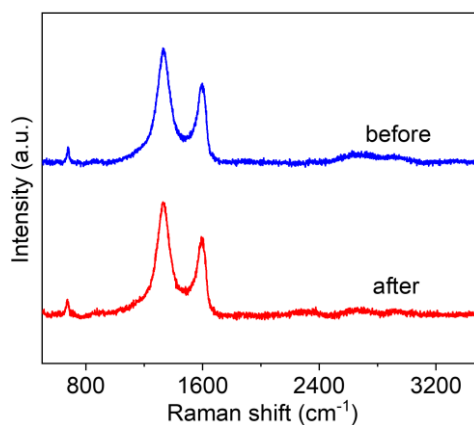


Figure S14. Raman spectra of S₁G-CoN₂ before and after the stability test.

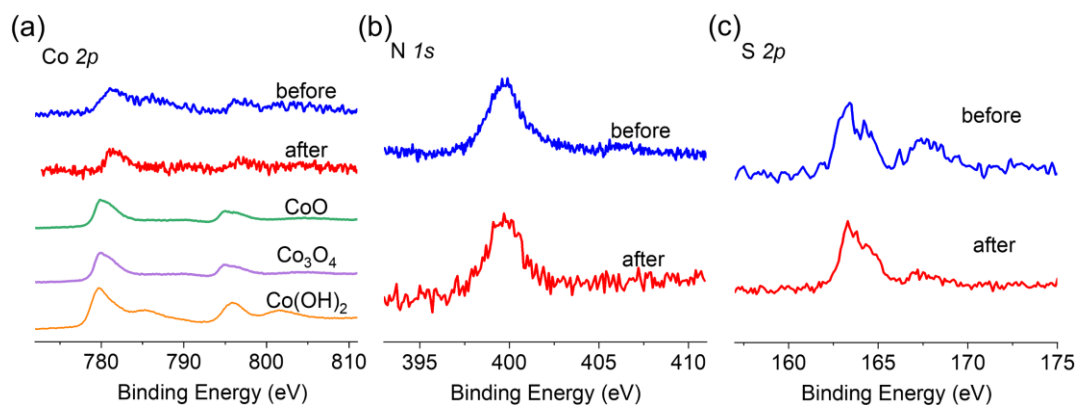


Figure S15. (a) Co 2*p* XPS surveys of S₁G-CoN₂ before and after the stability test, as well as those of reference materials. XPS surveys of S₁G-CoN₂ before and after the stability test in the N 1*s* (b) and S 2*p* (c) regions.

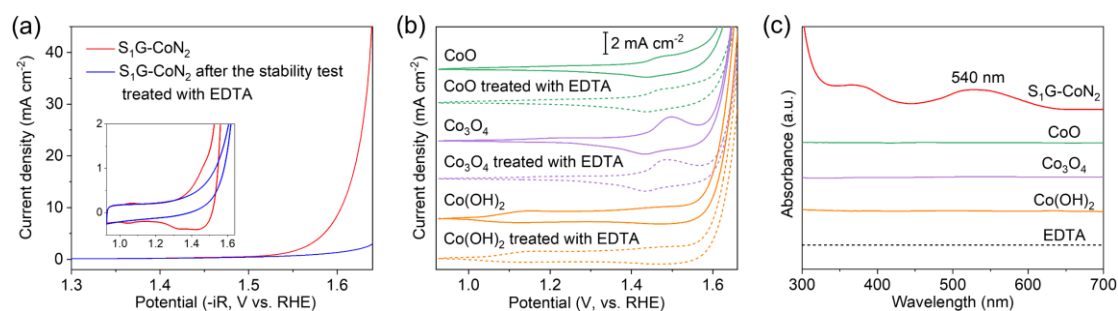


Figure S16. LSVs of S₁G-CoN₂ and S₁G-CoN₂ (after the stability test) treated with 0.5 M EDTA for 12 h, 1 M KOH. The inset shows the enlarged CVs of S₁G-CoN₂ and S₁G-CoN₂ (after the stability test) treated with 0.5 M EDTA solution. (b) CVs of other control samples before and after reacting with 0.5 M EDTA for 12 h. (c) UV-Vis spectra of EDTA solution reacted with S₁G-CoN₂ (after the stability test) and other control samples.

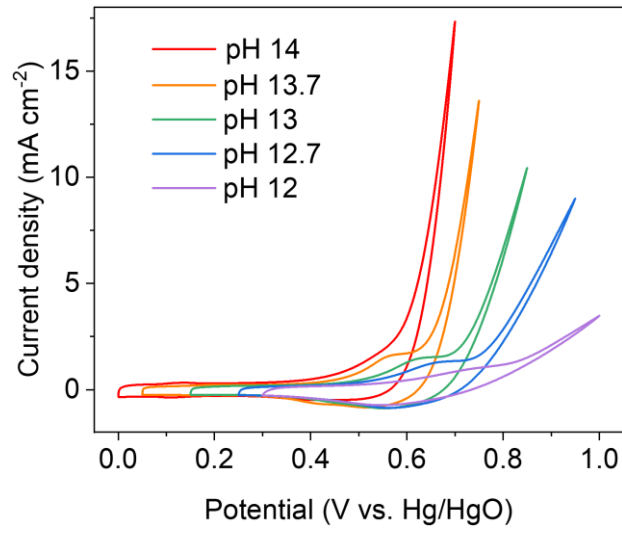


Figure S17. CVs of S₁G-CoN₂ measured in different KOH solutions with pH = 12, 12.7, 13, 13.7 and 14.

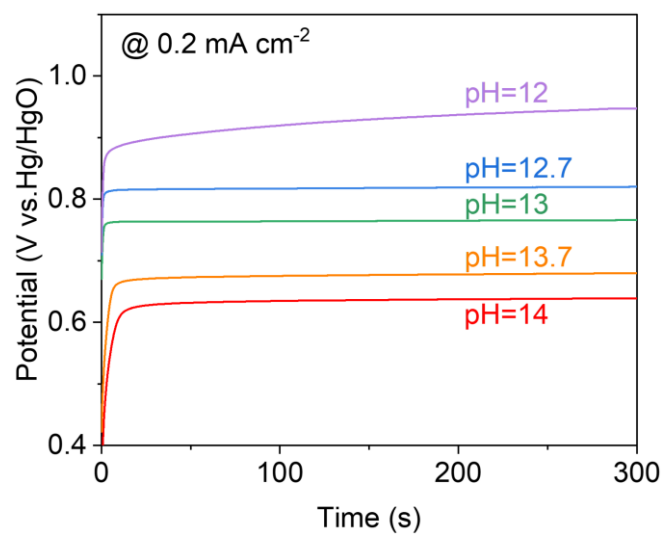


Figure S18. E-t curves of S₁G-CoN₂ measured at 0.2 mA cm⁻² in KOH solutions with different pH. The electrode was kept static in collecting the data.

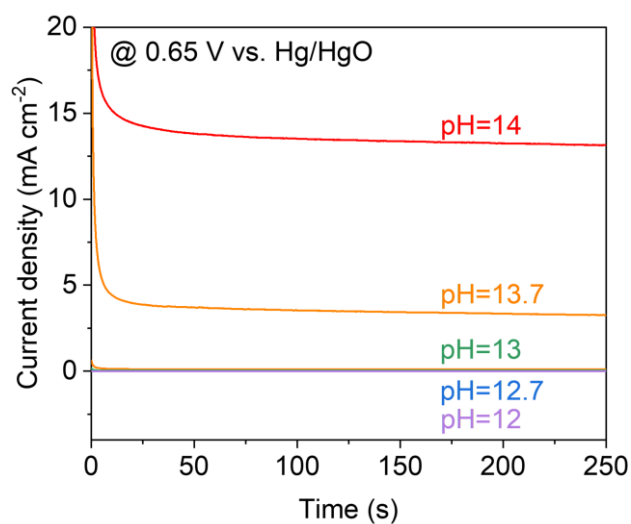


Figure S19. i-t curves of S₁G-CoN₂ measured at 0.65 V vs. Hg/HgO in KOH solutions with different pH. The electrode was kept static in collecting the data.

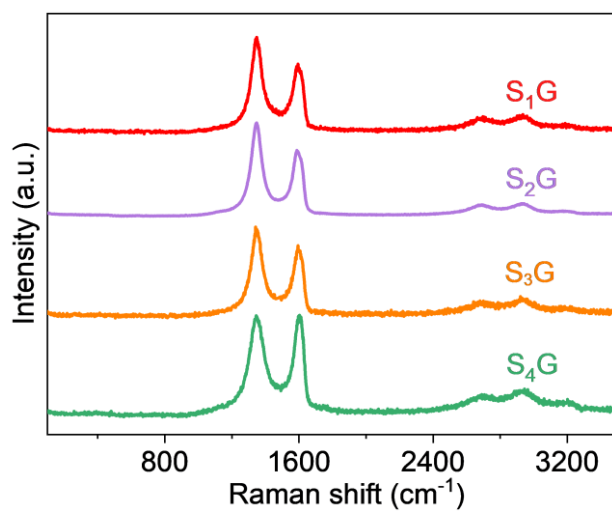


Figure S20. Raman spectra of S₁G, S₂G, S₃G and S₄G with a 532 nm laser.

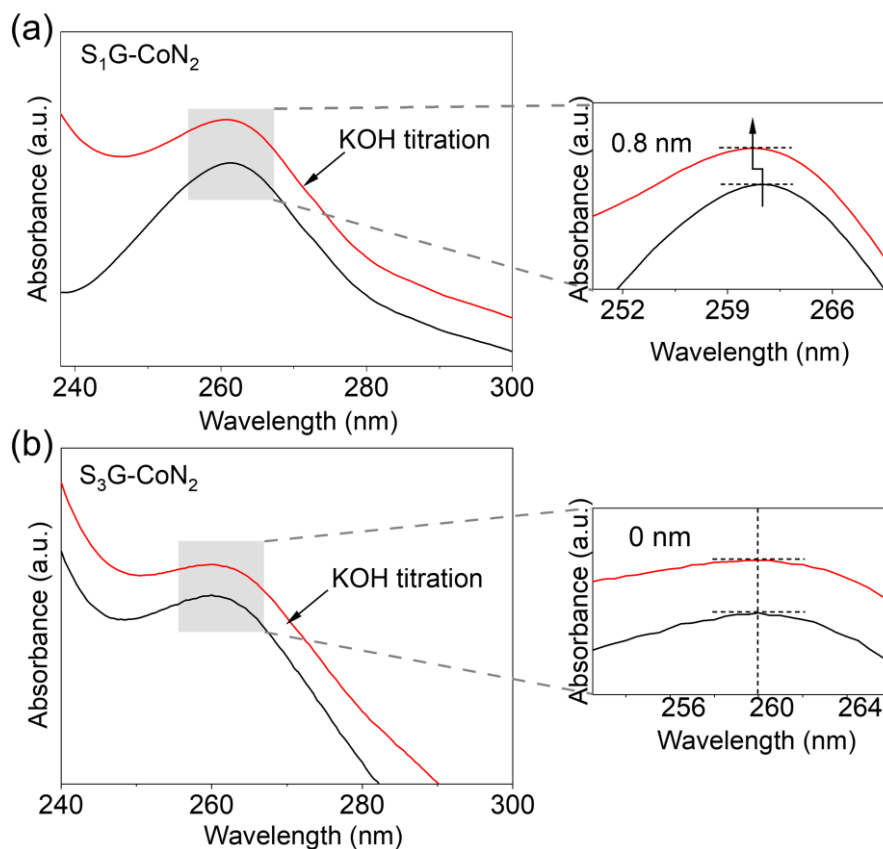


Figure S21. UV-Vis spectra of S₁G-CoN₂ (a) and S₃G-CoN₂ (b) before and after KOH titration. The molar ratio of Co to titrated KOH was 1:1. The data were collected in isopropanol.

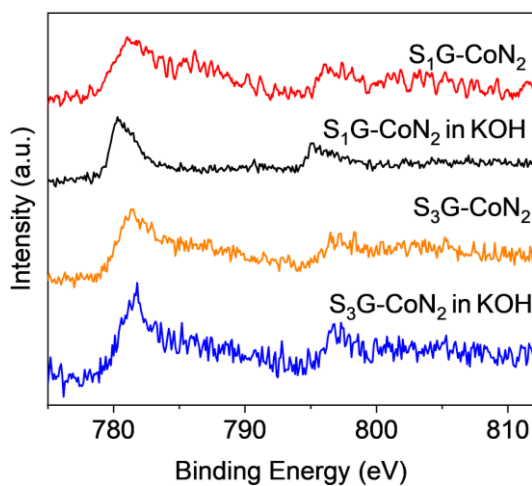


Figure S22. Co 2*p* core electron levels of S₁G-CoN₂ and S₃G-CoN₂ before and after being immersed into 1 M KOH solutions.

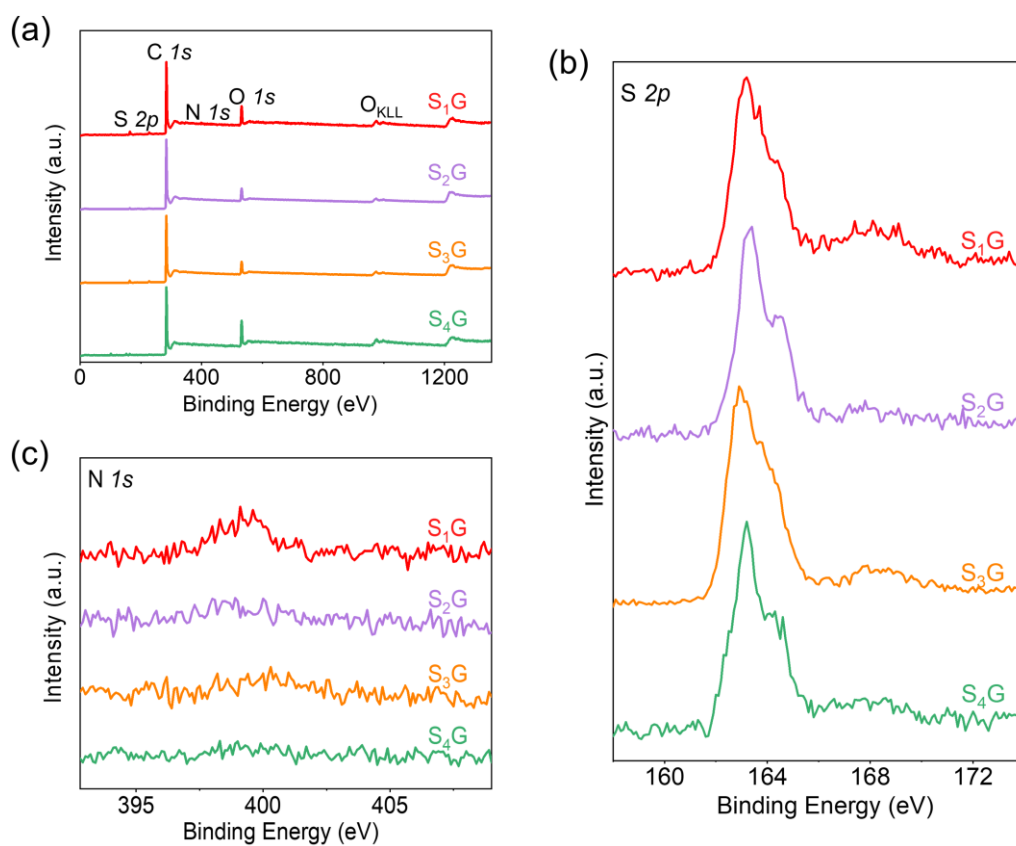


Figure S23. XPS overall surveys (a), S 2*p* (b) and N 1*s* (c) core electron levels of S₁G, S₂G, S₃G and S₄G.

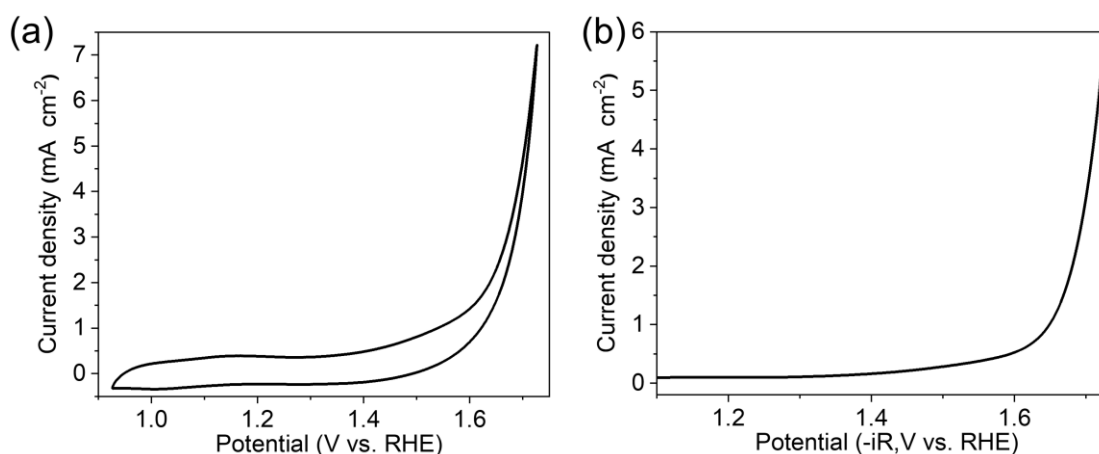


Figure S24. (a) CV of SNG-CoN₂. (b) LSV of SNG-CoN₂, 1 M KOH, 10 mV s⁻¹ scan rate, 1600 rpm. The potentials were compensated by 95% iR loss.

To synthesize SNG-CoN₂, GO (20 mg) was mixed with mercaptoacetic acid and urea (~ 1:50:50, mass ratio) in water/ethanol (10 ml/2.5 ml) under ultrasonication. Then the suspension was transferred into a PTFE lined stainless steel autoclave. It was sealed and kept at 150 °C for 3.5 h, and then washed with water and ethanol to obtain S/N-codoped graphene (SNG). The CoN₂ was mixed with SNG (1:1 mass ratio) in DMF and heated at 80 °C for 12 h. The final product is denoted as SNG-CoN₂.

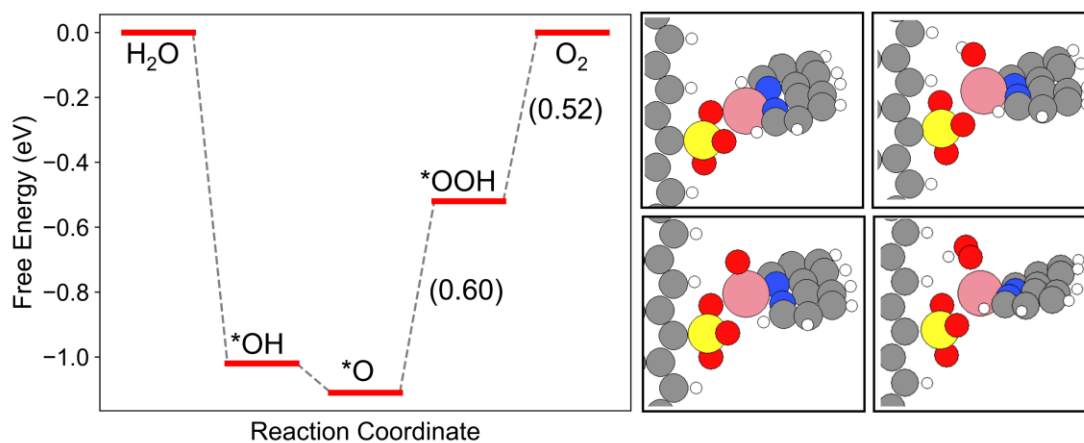


Figure S25. A free energy diagram of OER on the Co site of $\text{CoN}_2\text{O}_3\text{S}_1$ at $U=1.23$ V vs. RHE.

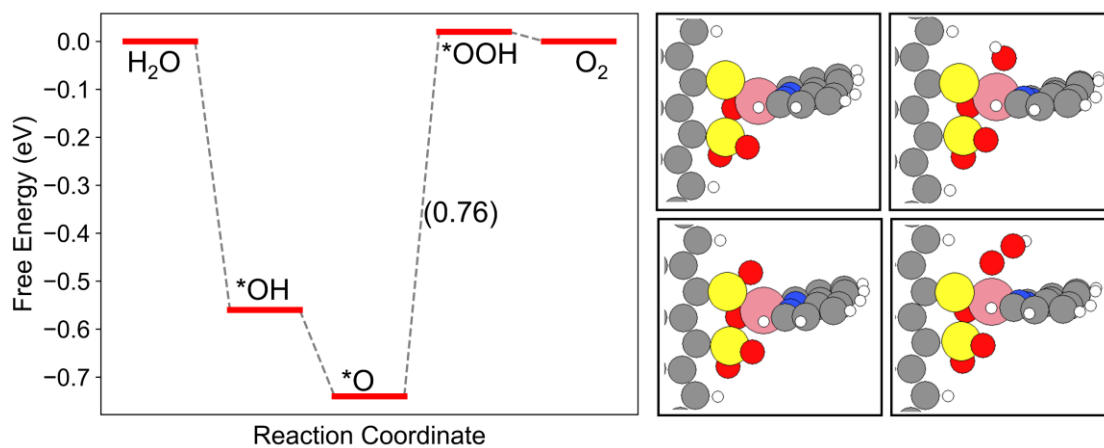


Figure S26. A free energy diagram of OER on the Co site of $\text{CoN}_2\text{O}_3\text{S}_2$ at $U=1.23$ V vs. RHE.

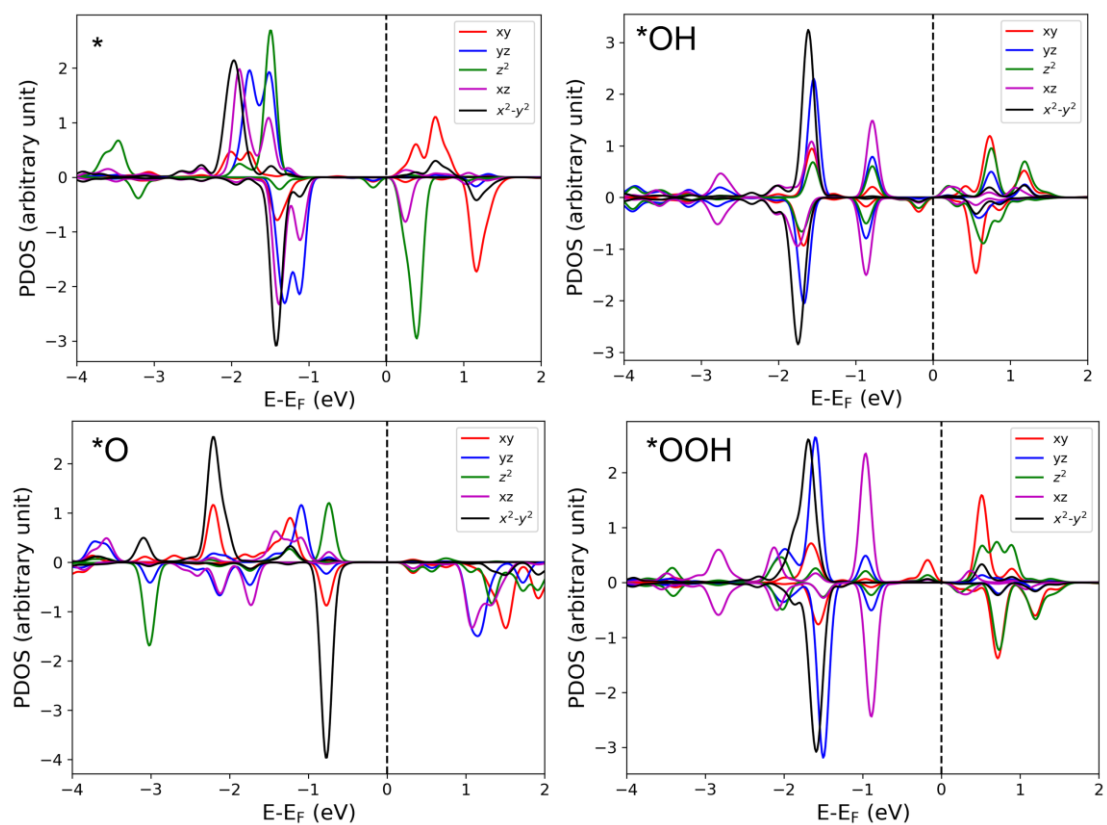


Figure S27. Density of states projected onto the d -orbitals of Co site in clean $\text{CoN}_2\text{O}_4\text{S}_1$ and those with adsorbed OER intermediates.

Table S1. The atomic contents of G, NG, S₁G, S₂G, S₃G and S₄G by elemental analysis.

	N at%	C at%	H at%	S at%	O at%
G	0.22	61.84	20.99	0.4	16.58
NG	4.99	53.59	24.30	0.6	16.96
S ₁ G	0.7	60.4	15.7	17.8	5.4
S ₂ G	0.1	78.6	12.7	0.3	8.3
S ₃ G	0.1	76.8	14.8	1.1	7.2
S ₄ G	-	67.3	19.8	1.5	11.4

Table S2. The total Co contents of OER electrocatalysts measured by ICP-OES.

Samples	Co content (mol mg_{support}⁻¹)
G-CoN ₂	2.8×10 ⁻⁶
NG-CoN ₂	4.2×10 ⁻⁶
S ₁ G-CoN ₂	3.0×10 ⁻⁶
S ₂ G-CoN ₂	3.0×10 ⁻⁶
S ₃ G-CoN ₂	2.3×10 ⁻⁶
S ₄ G-CoN ₂	3.4×10 ⁻⁶
G-CoN ₄	3.1×10 ⁻⁶
NG-CoN ₄	4.3×10 ⁻⁶
S ₁ G-CoN ₄	3.2×10 ⁻⁶
G-CoN ₆	2.9×10 ⁻⁶
NG-CoN ₆	4.2×10 ⁻⁶
S ₁ G-CoN ₆	3.1×10 ⁻⁶

The contained “mg_{support}” stands for the mass of graphene based solid supports, i.e., G, NG, S₁G, S₂G, S₃G and S₄G.

Table S3. EXAFS data fitting results of the S₁G-CoN₂.

Sample	Absorption edge	Path	R (Å)	CN	σ^2 (eV)	E ₀ (eV)	R
S ₁ G-CoN ₂	Co K-edge	Co-N	2.04	2.1	0.002	1.252	0.019
		Co-O	2.14	3.8	0.004		
		Co-S	2.73	1.3	0.010		

For Co K edge EXAFS spectra of the sample, the R_{bkg} is 1.0 Å, Fourier transform range of k is from 2.5-10.5 Å⁻¹ and R is from 1.0-2.75 Å. The amplitude reduction factor was determined by fitting a reference spectrum of the Co foil, and then it was used for fitting the Co K edge EXAFS spectra for these samples.

Table S4. The surface Co contents of OER electrocatalysts loaded on electrodes measured by ICP-OES.

Samples	Co contents (mol mg_{support}⁻¹)	Co contents (mol cm_{electrode}⁻²)
G-CoN ₂	4.2×10 ⁻⁷	2.0×10 ⁻⁸
NG-CoN ₂	5.7×10 ⁻⁷	2.6×10 ⁻⁸
S ₁ G-CoN ₂	4.2×10 ⁻⁷	2.9×10 ⁻⁸
S ₂ G-CoN ₂	3.4×10 ⁻⁷	1.5×10 ⁻⁸
S ₃ G-CoN ₂	2.3×10 ⁻⁷	1.1×10 ⁻⁸
S ₄ G-CoN ₂	2.6×10 ⁻⁷	1.5×10 ⁻⁸
G-CoN ₄	4.2×10 ⁻⁷	2.2×10 ⁻⁸
NG-CoN ₄	5.9×10 ⁻⁷	2.6×10 ⁻⁸
S ₁ G-CoN ₄	4.7×10 ⁻⁷	3.0×10 ⁻⁸
G-CoN ₆	3.8×10 ⁻⁷	2.8×10 ⁻⁸
NG-CoN ₆	5.5×10 ⁻⁷	2.4×10 ⁻⁸
S ₁ G-CoN ₆	4.2×10 ⁻⁷	2.2×10 ⁻⁸

The contained “mg_{support}” stands for the mass of graphene based solid supports, i.e., G, NG, S₁G, S₂G, S₃G and S₄G.

Table S5. TOF comparison of various reported non-noble metal OER electrocatalysts.

Catalyst	Electrolyte	Potential (V)	TOF (s⁻¹)	Ref.
S ₁ G-CoN ₂	1 M KOH	1.58	0.38	This work
SNG-Co ²⁺	1 M KOH	1.58	0.266	9
CoO _x -ZIF	1 M KOH	1.55	0.082	10
γ-CoOOH NS	1 M KOH	1.57	0.09	11
CoMM	1 M KOH	1.65	0.37	12
Co ₃ O ₄ /graphene	1 M KOH	1.63	0.554	13

Reference

1. N. Troullier and J. L. Martins, *Phys. Rev. B*, 1991, **43**, 1993-2006.
2. J. J. Mortensen, L. B. Hansen and K. W. Jacobsen, *Phys. Rev. B*, 2005, **71**, 035109.
3. S. R. Bahn and K. W. Jacobsen, *Comput. Sci. Eng.*, 2002, **4**, 56-66.
4. J. Wellendorff, K. T. Lundgaard, A. Møgelhøj, V. Petzold, D. D. Landis, J. K. Nørskov, T. Bligaard and K. W. Jacobsen, *Phys. Rev. B*, 2012, **85**, 235149.
5. J. K. Nørskov, J. Rossmeisl, A. Logadottir, L. Lindqvist, J. R. Kitchin, T. Bligaard and H. Jónsson, *J. Phys. Chem. B*, 2004, **108**, 17886-17892.
6. H. Wan, T. M. Østergaard, L. Arnarson and J. Rossmeisl, *ACS Sustainable Chem. Eng.*, 2019, **7**, 611-617.
7. W. Yuan, S. Wang, Y. Ma, Y. Qiu, Y. An and L. Cheng, *ACS Energy Lett.*, 2020, **8**, 692-700.
8. H. Zhong, K. H. Ly, M. Wang, Y. Krupskaya, X. Han, J. Zhang, J. Zhang, V. Kataev, B. Büchner, I. M. Weidinger, S. Kaskel, P. Liu, M. Chen, R. Dong and X. Feng, *Angew. Chem. Int. Ed.*, 2019, **58**, 10677-10682.
9. J. Wang, X. Ge, Z. Liu, L. Thia, Y. Yan, W. Xiao and X. Wang, *J. Am. Chem. Soc.*, 2017, **139**, 1878-1884.
10. S. Dou, C. L. Dong, Z. Hu, Y. C. Huang, J. I. Chen, L. Tao, D. Yan, D. Chen, S. Shen, S. Chou and S. Wang, *Adv. Funct. Mater.*, 2017, **27**, 1702546.
11. J. Huang, J. Chen, T. Yao, J. He, S. Jiang, Z. Sun, Q. Liu, W. Cheng, F. Hu, Y. Jiang, Z. Pan and S. Wei, *Angew. Chem. Int. Ed.*, 2015, **54**, 8722-8727.
12. P. Kumar, K. Kannimuthu, A. S. Zeraati, S. Roy, X. Wang, X. Wang, S. Samanta, K. A. Miller, M. Molina, D. Trivedi, J. Abed, M. A. Campos Mata, H. Al-Mahayni, J. Baltrusaitis, G. Shimizu, Y. A. Wu, A. Seifitokaldani, E. H. Sargent, P. M. Ajayan, J. Hu and M. G. Kibria, *J. Am. Chem. Soc.*, 2023, **145**, 8052-8063.
13. M. Leng, X. Huang, W. Xiao, J. Ding, B. Liu, Y. Du and J. Xue, *Nano Energy*, 2017, **33**, 445-452.